Dynamical and field effects in polymer-dispersed liquid crystals: Monte Carlo simulations of NMR spectra

C. Chiccoli,[1] P. Pasini,[1] G. Skačej,[2] C. Zannoni,[3] and S. Žumer[2]

[1]*Istituto Nazionale di Fisica Nucleare, Sezione di Bologna, Via Irnerio 46, I-40126 Bologna, Italy*
[2]*Physics Department, University of Ljubljana, Jadranska 19, SI-1000 Ljubljana, Slovenia*
[3]*Dipartimento di Chimica Fisica ed Inorganica, Università di Bologna, Viale Risorgimento 4, I-40136 Bologna, Italy*

We analyze the dynamical aspects of molecular ordering in nematic droplets with radial and bipolar boundary conditions—as encountered in polymer-dispersed liquid crystals—by calculating and interpreting the corresponding ^{2}H NMR spectra. In particular, we focus on effects of molecular motion such as fluctuations of molecular long axes and translational diffusion, and on external field ordering effects. As in our previous paper [Phys. Rev. E **60**, 4219 (1999)], where field effects were not considered, equilibrium configurations inside nematic droplets are obtained from Monte Carlo simulations of the Lebwohl-Lasher lattice spin model.

I. INTRODUCTION

Polymer-dispersed liquid crystals (PDLC) are materials consisting of microscopic nematic droplets embedded in a polymer matrix [1]. With characteristic radii from a few tens of nanometers to well above a micron (see Fig. 1), these systems are rather important for investigations of the liquid crystalline behavior in a confined environment. The nematic structure inside PDLC droplets depends on the polymer matrix itself and on the surface preparation method, resulting in different types of surface boundary conditions: radial [2,3] or axial [3] for homeotropic surface anchoring and toroidal [4] or bipolar [2,3,5] for tangential anchoring. Applying an external electric or magnetic field, additional ordering effects can be observed [2,5]. These field-induced effects turn out to be of great importance for technical applications—mainly for the design of optical devices, such as switchable windows, displays, or fast light shutters. Apart from elastic continuum approaches [1], Monte Carlo (MC) computer simulations performed on lattice model systems have been widely used to investigate PDLC theoretically [6]. Indeed, the MC technique was shown to be a powerful method also for the simulation of experimental observables, like polarized light textures or NMR spectra [7]. Recently, we have developed a method for calculating NMR spectra that is applicable also in the presence of significant molecular motion [8]. In the present paper, we extend the analysis presented in Ref. [8] and include aligning effects of external (electric or magnetic) fields. As in Ref. [8], we start by simulating nematic configurations inside PDLC droplets for different (radial and bipolar) boundary conditions using the MC simulation technique and then interpret the simulation results through NMR spectra. Thereby we investigate the competition between nematic ordering effects, surface anchoring, and the external field. Note that analyses in Refs. [9,10] already deliver thorough studies of external field effects in radial and bipolar droplets and contain the corresponding NMR spectra, but none of these studies presents a calculation of the spectra in the presence of significant molecular motion. This paper is organized as follows: we first briefly recall some features of

the Monte Carlo simulation and the calculation of the spectra (for more details the reader is referred to Ref. [8] and to references therein); then we examine the calculated spectra and, finally, discuss field-induced ordering effects in PDLC droplets.

II. MONTE CARLO SIMULATIONS AND CALCULATION OF NMR SPECTRA

The computer simulations employed here to simulate the nematic liquid crystal are based on a simple model system introduced by Lebwohl and Lasher several years ago [11]. In this model uniaxial nematic molecules (or, equivalently, close-packed molecular clusters [6,10]) are represented by ''spins'' arranged into a simple cubic lattice. Thereby more particles than in off-lattice models can be treated and, despite the lattice restriction, the orientational behavior of molecules is reproduced sufficiently well. In the presence of an external field, the Hamiltonian for our model system consisting of N spins can be written as

$$U_N = -\epsilon \sum_{\langle i<j \rangle} P_2(\cos\beta_{ij}) - \epsilon\eta \sum_{i=1}^{N} P_2(\cos\beta_i), \quad (1)$$
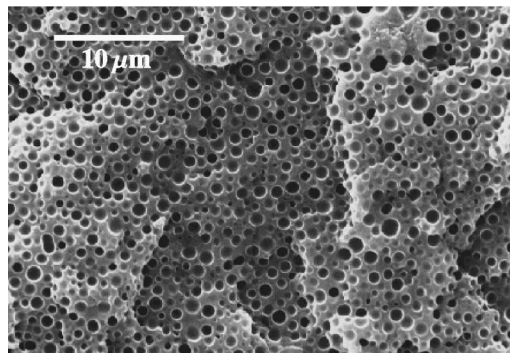

FIG. 1. Scanning electron microscope photograph of a PDLC sample with the liquid crystal removed [13]. The average droplet radius is equal to ~400 nm.

with P_2 standing for the second-rank Legendre polynomial given by $P_2(x) = (3x^2 - 1)/2$, $\cos \beta_{ij} = \mathbf{u}_i \cdot \mathbf{u}_j$, and $\cos \beta_i = \mathbf{f} \cdot \mathbf{u}_i$, where $\mathbf{f}$ and $\mathbf{u}_i$ are unit vectors giving the orientation of the external field and of the spin located at the ith lattice site, respectively. In Eq. (1) the first sum goes over nearest neighbors only and favors parallel molecular alignment, while the second one simulates the coupling with the field. Further, ϵ and η are constants describing the strengths of the intermolecular interaction and of the coupling with the external field, respectively. In the magnetic field case the dimensionless constant η is defined by $\epsilon \eta = \chi_a V_0 B^2 / 3\mu_0$, where B stands for the magnetic induction, $\chi_a = \chi_{||} - \chi_{\perp}$ is the anisotropy of the microscopic magnetic susceptibility (|| and $\perp$ referring to the direction of $\mathbf{u}_i$); μ_0 the permittivity of the vacuum, and V_0 the volume of space belonging to one molecule or spin (see, e.g., [9]). For $\eta > 0$ ($\chi_a > 0$) nematic molecules (spins) are aligned along $\mathbf{f}$. In order to influence the molecular alignment inside the droplet significantly, the external field has to be strong enough so that the characteristic length of the field-induced distortion (i.e., the magnetic coherence length $\xi \propto 1/B$ [12]) becomes comparable to or smaller than the characteristic dimension of the confined system, in our case simply the droplet radius R. In an experiment with an aligning magnetic field it is usually the NMR spectrometer field itself taking the role of the external field introduced in the Hamiltonian (1). Here, however, we still distinguish between the ''weak'' NMR spectrometer field and the ''strong'' external field of variable strength, responsible for the additional molecular alignment. Note that although above we decided to refer to magnetic-field effects, in a real experiment one can more easily achieve the high field strengths required to align nematic molecules by applying an electric field [5,12,13]. Matching aligning effects in the electric and the magnetic case, for a given nematic species one can translate any magnetic-field strength (or B) into an equivalent strength of the electric field (E) [9]. In the electric case we then have $\epsilon \eta = \epsilon_a \epsilon_0 V_0 E^2 / 3$, where $\epsilon_a = \epsilon_{||} - \epsilon_{\perp}$ is the microscopic anisotropy of the dielectric constant and ϵ_0 the dielectric constant of the vacuum.

To model a PDLC droplet we carve a ''jagged'' sphere of radius R from the cubic lattice. The interaction of nematic molecules with the surrounding polymer is modeled by an additional layer of spins (''ghosts'') whose orientations are fixed and chosen in accordance with the desired (radial or bipolar) boundary conditions [14–16]. For simplicity, the strength of the nematic-ghost interaction is chosen to be equal to that of the nematic-nematic one. This implies that in cases corresponding to the nematic phase in our simulation the surface anchoring extrapolation length [12] is of the order of a few spin-to-spin spacings on the lattice [17]. As reported in [6,10], a single spin can represent a cluster of up to 100 nematic molecules (of volume ~ 1 nm^3 each), and therefore the spin-to-spin spacing can be estimated by $\lesssim 5$ nm. Consequently, the extrapolation length lies around 10 nm, while its experimental values usually range between 100 nm and 10 μm (only exceptionally down to 10 nm) [18]. Therefore, in our case surface anchoring should be regarded as rather strong.

Monte Carlo simulations are now performed as follows. The calculation at the lowest temperature starts from a perfectly ordered configuration depending on boundary conditions. At higher temperatures, however, it starts from an already equilibrated configuration at the nearest lower temperature, if this is available. Then the Metropolis scheme [19] is employed to perform updates in spin orientations [20,21]. The rejection ratio was chosen to be close to 0.5 in order to ensure an adequate evolution of the spin system. Once the system is equilibrated, 1024 spin configurations are stored and used as input for the calculation of NMR spectra. For both types of boundary conditions the number of particles (spins) inside the droplet was set to 5832, whereas the additional surface layer fixing the boundary conditions contains 1352 spins.

The output from our MC simulation consists of a set of thermodynamic observables (energy, order parameters, and correlation functions) and of full sets of ''spin coordinates'' and their direction cosines. It is possible to analyze these detailed configuration data by looking at snapshots of molecular organizations (e.g., [7]), or by relating them directly to experimental observables. In this latter case it is interesting to calculate ^{2}H NMR spectra. This experimental method is advantageous since it only yields information on the deuterated nematic material and is applicable to submicron droplets where optical methods already fail to yield useful results. Further, NMR spectra give information both on orientational ordering and on molecular dynamics inside droplets. As such, deuterium NMR is widely used to investigate PDLC materials [2,13,22,23].

A ^{2}H NMR spectrum of a deuterated nematic in the bulk isotropic phase consists of a single narrow line (line width below 100 Hz) placed into the spectrum according to the Zeeman splitting of deuteron energy levels in the spectrometer magnetic field $\mathbf{B}_0$. There is an additional perturbative contribution to these energy levels originating from quadrupolar interactions between deuterons and the electric field gradient (EFG) of the C-^{2}H bonds in nematic molecules. Contrary to the isotropic phase, in the nematic phase this perturbation is not averaged out by molecular motions. Consequently, in an undistorted sample the single narrow line splits into a doublet whose frequency splitting is given by [1,24,25]

$$\omega_Q = \pm \, \delta \omega_Q \, S \left(\frac{3 \cos^2 \theta - 1}{2} \right). \qquad (2)$$

Here θ stands for the angle between the nematic director $\mathbf{n}$ (i.e., the average molecular orientation) and the direction of the NMR spectrometer magnetic field, S is the scalar order parameter defined by the ensemble (or time) average $S = \langle [3(\mathbf{n} \cdot \mathbf{u}_i)^2 - 1]/2 \rangle_i$ [12], and $\delta \omega_Q$ is the quadrupolar coupling constant ($\delta \omega_Q / 2\pi \sim$ several 10 kHz). Note that in Eq. (2) we have assumed that the effective EFG tensor averaged over fast molecular rotations around the molecular long axis is uniaxial and, further, that biaxiality in the molecular ordering itself can be neglected as well.

In confined nematics such as PDLC we have $\mathbf{n} = \mathbf{n}(\mathbf{r})$ and $S = S(\mathbf{r})$, depending on the boundary conditions imposed by the polymer matrix. Consequently, superimposing molecular contributions given by Eq. (2) from all over the sample, each boundary condition type results in a specific spectrum. This identification becomes, however, more difficult when translational diffusion of molecules is not negligible [8]. If motional effects such as fluctuations of molecular long axes or

translational diffusion are to be taken into account when the spectra are calculated, it is convenient to use a semiclassical approach with the time-dependent deuteron spin Hamiltonian [25]. The spectrum $I(\omega)$ is then given by the Fourier transform of the relaxation function $G(t)$, i.e., by $I(\omega) = \int \exp(i\omega t) G(t) dt$, where $G(t)$ is generated as

$$G(t) = \exp(i\omega_Z t) \left\langle \exp\left(i \int_0^t \Omega_Q[\mathbf{r}_i(t'),t'] \, dt' \right) \right\rangle_i, \quad (3)$$

with $\Omega_Q[\mathbf{r}_i(t),t] = \pm \delta\omega_Q [3(\mathbf{u}_i \cdot \mathbf{B}_0/B_0)^2 - 1]/2$ and $\mathbf{u}_i$ standing for the ''instantaneous'' orientation of the ith molecule (spin). Further, in Eq. (3) ω_Z denotes the Zeeman resonance frequency, while the brackets $\langle \cdots \rangle_i$ represent an ensemble average over molecules in the sample.

As already indicated above, the instantaneous molecular (or spin) orientations $\mathbf{u}_i$ are obtained from the MC simulation output data and fluctuate during the MC evolution process. In contrast to molecular dynamics simulations, the corresponding dynamics is determined by the arbitrary evolution process generated by the Metropolis algorithm. Though, this evolution simulates the ''natural'' one sufficiently well, as discussed in [8]. On the other hand, translational diffusion is simulated by a simple random-walk process in which molecules jump between neighboring lattice sites, always adjusting their orientation to the local and instantaneous $\mathbf{u}_i$. Both types of motional effects thus affect the instantaneous resonance frequency $\omega_Z + \Omega_Q[\mathbf{r}_i(t),t]$, thereby leaving a signature in the relaxation function $G(t)$ and, consequently, in the NMR line shape $I(\omega)$.

In the following we are going to review NMR spectra of PDLC droplets in the nematic and in the isotropic phase, studying cases in an external field for different values of the field strength (and η). Two translational diffusion regimes will be considered: the slow and the fast diffusion regime (note that the intermediate regime has been examined in Ref. [8] for $\eta = 0$). In the first case, translational diffusion can be ignored completely; then the only relevant molecular motion are the fluctuations of $\mathbf{u}_i$. In the second case, the molecular diffusive motion (assumed isotropic) is fast in comparison with the characteristic NMR time scale $t_0 \sim \omega_Q^{-1} \sim (\delta\omega_Q S)^{-1}$ [see Eq. (2)]. In other words, a molecule must diffuse far enough to change its orientation significantly—in a droplet this distance is given by its radius R—in a characteristic time shorter than the NMR time scale. Therefore, in small droplets, diffusion is expected to be more important than in the large ones. However, since $t_0 \propto S^{-1}$, diffusive effects can become important also in those regions of large droplets where S is small.

The degree of diffusional averaging can be quantified by introducing the dimensionless parameter $e = \omega_Q R^2/12\pi D$ [2], where D is the effective diffusion constant and ω_Q is given by Eq. (2). In cases without (or with very slow) diffusion we have $e \to \infty$, while in the fast diffusion regime, $e \to 0$ holds. The transition between the two regimes occurs for $e \approx 1$. The actual value of e can be deduced from simulation parameters and is, in cases we claim to correspond already to the fast diffusion regime, equal to $e \approx 0.45$. Here we assumed that most molecules are aligned along the external field direction and that the nematic order is homogeneous

with $S = 0.8$ throughout the droplet. Note that although $e \ll 1$ is still not fulfilled, the translational diffusion is already significant and the resulting NMR spectra show features of diffusive motional averaging. Increasing the diffusion rate (decreasing e) even further results only in an additional decrease of the spectral line width, while the spectral shape is maintained. On the other hand, translational diffusion is seen to affect NMR spectra only negligibly for $e \gtrsim 14$ [8]. Choosing specific values for $\delta\omega_Q$ and D, it is possible to rewrite both bounds for e in terms of the droplet radius R. Hence, putting $\delta\omega_Q \approx 2\pi \times 40$ kHz, $D \approx 4 \times 10^{-11}$ m^2/s (e.g., for bulk 5CB at room temperature) [1], and again $S \approx 0.8$, we find that the spectra of droplets smaller than $R \approx 60$ nm are already averaged by diffusion, while diffusive motions can be ignored in droplets larger than $R \approx 330$ nm. However, here it is again necessary to stress that a single spin in our simulation can represent a cluster of up to 100 nematic molecules and that because the number of spins in the simulation is limited, we can only access droplet radii below ~ 60 nm. In this range of R the simulation is meaningful and, for the above values of $\delta\omega_Q$ and D, we are actually always in the fast diffusion regime.

Reviewing actual PDLC samples, one encounters a rather broad distribution of droplet sizes, the lower bound for their diameter being several tens of nanometers (e.g., 20 nm [22]), and the upper well above 1 μm. This indicates that despite the smallness of the simulated droplets they already are realistic. Increasing the number of spins inside the droplet, however, does not change the main qualitative features of our results; therefore, we have chosen the compromise to simulate a wider range of field strengths and temperatures for smaller droplets. Consequently, the NMR spectra become rather ''noisy'' due to a relatively small number of spins inside one droplet. Then, for smoothening, a convolution with a Gaussian kernel of width $0.04\,\delta\omega_Q$ has been performed. For further details concerning the calculation of the spectra and the characteristic time scales related to molecular motion, see Refs. [8,26].

III. RESULTS

A. Spectra below nematic-isotropic transition: Bipolar droplet

Consider the bipolar case first. The local anchoring easy axis is now directed tangentially to the local droplet surface, while it is also lying in a plane containing the droplet symmetry axis [see Fig. 3(b), inset]. Suppose also that the directions of the NMR spectrometer field and of the external field match with the symmetry axis of the droplet, here denoted by z. For all droplets in a real PDLC sample this can be achieved by exposing the sample to an external magnetic field of sufficient strength during the droplet formation process [2]. Consider now the limit without translational diffusion and assume also that there is no external field applied ($\eta = 0$), except for the weak spectrometer field that anyway does not disturb the nematic director configuration. The reduced temperature $T^* = k_B T/\epsilon$ was set to $T^* = 0.8$ to assure the existence of the nematic phase inside the droplet (just recall that the nematic-isotropic transition occurs at $T_{NI}^* = 1.1232$ for the Lebwohl-Lasher model [20] and that T_{NI}^* is slightly reduced to around 1 for a bipolar droplet without any
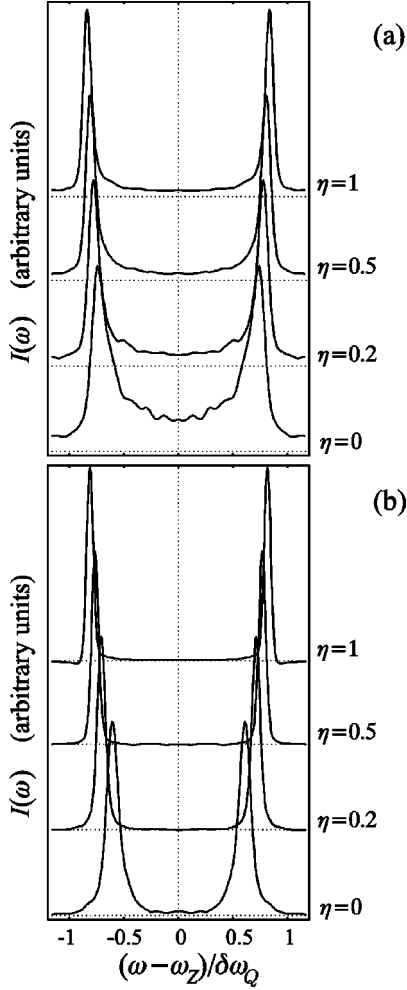
FIG. 2. ^{2}H NMR spectra of the bipolar droplet in the nematic phase at $T^*=0.8$ for different values of the external field strength ($\propto \sqrt{\eta}$); no-diffusion limit (a), fast diffusion limit (b). The quadrupolar splitting increases with increasing η. All spectra have been normalized so as to obtain same peak heights.

field applied [10]). The results show that a considerable portion of nematic molecules—especially those in the droplet core—is directed approximately along the spectrometer field, which results in a spectrum consisting of two well-defined peaks [Fig. 2(a)] situated almost at maximum quadrupolar splitting $\delta\omega_Q$, reduced by the factor S due to fluctuations of molecular long axes [see Eq. (2)]. These peaks are located at $\omega_Q/\delta\omega_Q\approx\pm(0.73\pm0.01)$, which roughly suggests that $S\approx0.73$. Unless noted otherwise, the error in S arising from the determination of peak positions in all following cases equals ±0.01. On the other hand, one can deduce the value of the scalar order parameter S also directly from the MC data by diagonalizing the time- (rather than ensemble-) averaged ordering matrices for each of the spins, identifying the largest eigenvalues as the local S [27], and then averaging these local S over the whole droplet to obtain the overall S. In our case such an estimate yields $S\approx0.76\pm0.04$. The local S are position dependent and the variance given here for the overall S originates in the ensemble average over these local S. Note that the agreement of the two estimates for S is rather good.

Increasing now the external field strength to yield $\eta=0.2$, the two peaks in the spectrum move toward larger

TABLE I. Bipolar droplet at $T^*=0.8$: comparison of S and $\langle\omega_Q\rangle$ deduced from NMR spectra (peak) with those calculated directly from Monte Carlo data (MC).

η	S_{peak}	S_{MC}	$(\langle\omega_Q\rangle/\delta\omega_Q)_{peak}$	$(\langle\omega_Q\rangle/\delta\omega_Q)_{MC}$
0.0	0.73 ± 0.01	0.76 ± 0.04	0.61	0.59
0.2	0.78 ± 0.01	0.79 ± 0.03	0.71	0.70
0.5	0.81 ± 0.01	0.81 ± 0.02	0.76	0.77
1.0	0.84 ± 0.01	0.84 ± 0.015	0.82	0.82

$|\omega_Q|$, i.e., to $\omega_Q/\delta\omega_Q\approx\pm0.78$ and become narrower. The MC data now yield $S\approx0.79\pm0.03$. As it is evident from Fig. 2(a), this trend continues also in even stronger fields with $\eta=0.5$ ($\omega_Q/\delta\omega_Q\approx\pm0.81$) and $\eta=1.0$ ($\omega_Q/\delta\omega_Q\approx\pm0.84$). The corresponding MC-data values for S are then 0.81 ± 0.02 and 0.84 ± 0.015, agreeing perfectly with the values deduced from the spectra (see also Table I). Note that already for $\eta=0.2$ the external field is extremely strong: considering the magnetic case and taking $\epsilon=k_BT_{NI}/1.1232\approx0.023$ eV (with $T_{NI}\approx300$ K), the macroscopic anisotropy of the magnetic susceptibility $\chi_aS\approx10^{-6}$, and assuming a single spin to represent a cluster of up to 100 nematic molecules of volume 1 nm^3 each, we obtain as much as $B\approx150$ T. If we used an electric instead of the magnetic field to align the nematic, the corresponding field strength for a typical liquid crystal with $\epsilon_aS\approx1$ and for same η would be ≈45 V/μm, which is—like in the magnetic case—rather difficult to be implemented experimentally. It must be stressed, however, that strong external fields are required to induce a detectable distortion because the simulated droplet is still rather small and because surface anchoring was chosen as strong, as noted in Sec. II.

To gain more insight into field-induced changes of NMR spectra, it is convenient to divide the PDLC droplet into onionlike spherical layers (shells) of equal thickness and investigate nematic ordering layer by layer [14]. For this purpose we calculate the standard nematic order parameter S and the external field order parameter $\langle P_2\rangle_B$ in each layer. The parameter S is again obtained by diagonalizing the local ordering matrices, as described above. It gives information on the degree of nematic ordering with respect to the average local molecular direction (the local director $\mathbf{n}$). The parameter $\langle P_2\rangle_B$, however, is defined as $\langle P_2\rangle_B=\langle\frac{1}{2}(3\cos^2\beta_i-1)\rangle_i$, with $\cos\beta_i=\mathbf{f}\cdot\mathbf{u}_i$ and the brackets $\langle\cdots\rangle_i$ representing the time and ensemble average over orientations of molecules (spins) within a given spherical layer. Contrary to S, $\langle P_2\rangle_B$ contains information on molecular ordering along a fixed direction—determined by the external field—and thereby reflects also spatial variations of the nematic director. Note also that the number of spins within a certain shell increases rapidly when moving from the droplet center toward the surface (from 8 spins in the 1st shell to 1392 spins in the 11th). Despite this, the variance of S (calculated from the ensemble average over spins within a given shell) is not highest for the innermost shells. In the nematic phase, for example, it never exceeds 3% in the central shell containing 8 molecules only. The maximum variance (up to 6% in the bipolar and up to 30% in the radial case) usually occurs in intermediate shells or even close to the substrate. In these
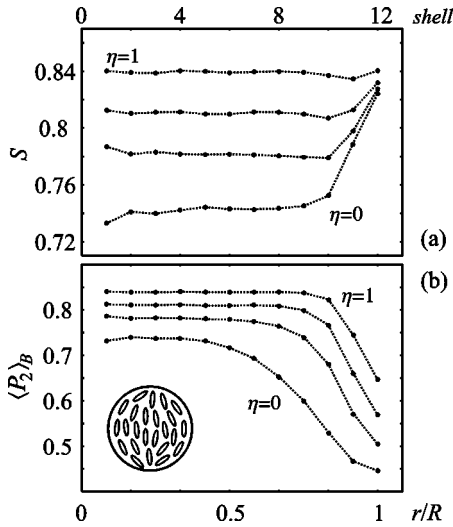
FIG. 3. Order parameters calculated for the bipolar droplet at $T^*=0.8$ (nematic phase): (a) standard nematic (S) and (b) external field ($\langle P_2\rangle_B$) order parameter as a function of the distance from the droplet center. Curves are plotted for (top to bottom): $\eta=1$, $\eta=0.5$, $\eta=0.2$, and $\eta=0$, respectively. External field enhances the degree of nematic ordering (a) and increases the size of the aligned core (b). The molecular alignment for $\eta=0$ is depicted schematically as inset.

regions, aligning effects of the substrate conflict either with the aligning effect of the external field or with the parallel aligning tendency of the nematic-nematic interaction. The competition of these effects may result also in a slight decrease of S.

The values of S for the bipolar droplet in the nematic phase for $T^*=0.8$ are displayed in Fig. 3(a). They indicate that the degree of nematic ordering is almost constant throughout the droplet core with $S\approx0.74$ when the external field is absent, while it increases to $S\approx0.82$ in the surface layer due to ordering effects of the polymer substrate. Applying the field, the degree of molecular order inside the core increases, if compared to the case without the field; e.g., for $\eta=1$ even to $S\approx0.84$. The profiles of the field order parameter $\langle P_2\rangle_B$ are plotted in Fig. 3(b). The corresponding curve for $\eta=0$ shows that in absence of the field there is already net molecular alignment along the z axis, which agrees with the imposed bipolar boundary conditions whose symmetry axis matches with z. The curves for $\eta>0$ show that with the increasing field strength more and more molecules (spins) orient along z (i.e., along $\mathbf{f}$), thereby increasing the size of the droplet core where the nematic liquid crystal is almost undistorted and $\mathbf{n}\|z$. The thickness of the distorted region is related to the external field coherence length ξ and is obviously microscopic because the applied field is extremely strong.

According to the above observations, the increase of the quadrupolar splitting ω_Q in strong fields can be attributed both to the overall increase in the local degree of ordering, i.e., to an increase of S—as observed also experimentally [28]—and to the additional molecular alignment along $\mathbf{f}$ resulting in an increase of $\langle P_2\rangle_B$; see formula (2). Also the narrowing of the spectral lines is related to the increase of $\langle P_2\rangle_B$ since in the droplet core the bipolar configuration is replaced by the "aligned" one. The spectral line narrowing

further follows from changes in the distribution of local $S(\mathbf{r})$. In fact, in strong fields the field-enhanced "bulk" value of S approaches the surface-induced value and thus the distribution of S becomes narrower.

Considering now Fig. 2(b) and the spectra of bipolar droplets in the fast translational diffusion limit (or, equivalently, in small enough nematic droplets), the spectra for all η still consist of two well-defined lines now positioned, however, at an average quadrupolar frequency given by $\langle\omega_Q\rangle=\pm\,\delta\omega_Q\langle\frac{1}{2}[3(\mathbf{u}_i\cdot\mathbf{B}_0/B_0)^2-1]\rangle_i$, where $\langle\cdots\rangle_i$ represents the average over fluctuations and diffusive motions of all molecules within the PDLC droplet [2,29]. The quantity $\langle\omega_Q\rangle$ can be calculated also directly from MC data and, according to values presented in Table I, the agreement with actual peak positions is very good.

B. Spectra below nematic-isotropic transition: Radial droplet

We now turn to radial droplets, i.e., droplets in which the polymer matrix favors normal (homeotropic) surface anchoring. In absence of external fields, for this kind of boundary condition the nematic director is directed radially from the droplet center, giving rise to a "hedgehog"-like structure [see Fig. 5(a), inset]. Then in the very vicinity of the center, the elastic deformation (splay) becomes rather strong and therefore it is convenient in this tiny region for the nematic to melt, i.e., to decrease the degree of nematic order (S) so as to reduce the elastic deformation free energy. In the rest of the droplet the radial alignment still exists and therefore in each of the intermediate and outer shells the spin orientations are distributed evenly through the whole solid angle. As far as NMR is concerned, this situation is equivalent to having a polycrystalline powder sample and, indeed, the spectrum of the radial droplet for $\eta=0$ is the Pake-type powder pattern consisting of two asymmetric peaks at $\pm\frac{1}{2}\delta\omega_Q S$ [25], as shown in Fig. 4(a) for the diffusionless case. A calculation of the nematic order parameter S [Fig. 5(a)] for $\eta=0$ shows that the value of S in the center of the droplet is nonzero but considerably smaller (≈0.32) than the value obtained in the intermediate and surface layers ($\gtrsim0.75$). This confirms the existence of a small (~4 molecular or "spin" dimensions diameter) and fairly disordered defect core.

Applying an external field with $\eta>0$, the radial "hedgehog" structure containing a point defect transforms into an axially symmetric structure with a ring defect. The degree of ordering in the center therefore increases significantly and the molecules of the core align along the field direction (compare with order parameters S and $\langle P_2\rangle_B$ plotted in Fig. 5). There is no critical field characterizing the transition between the "hedgehog" and the aligned structure: the size of the aligned core increases gradually with the increasing field strength [9]. This can be confirmed also by inspecting the resulting NMR spectra shown in Fig. 4(a). For strong external fields with $\eta\gtrsim0.2$ the Pake-type pattern transforms into a spectrum with two narrow peaks, similar to those observed for bipolar boundary conditions. Again, this indicates that for $\eta\gtrsim0.2$ most of the molecules are aligned along $\mathbf{f}$, except for those lying close enough to the polymer substrate. In fact, surface-induced radial order persists in the outermost molecular layers, which results in a strong decrease of the order parameter $\langle P_2\rangle_B$ [Fig. 5(b)] in the surface region. The thick-
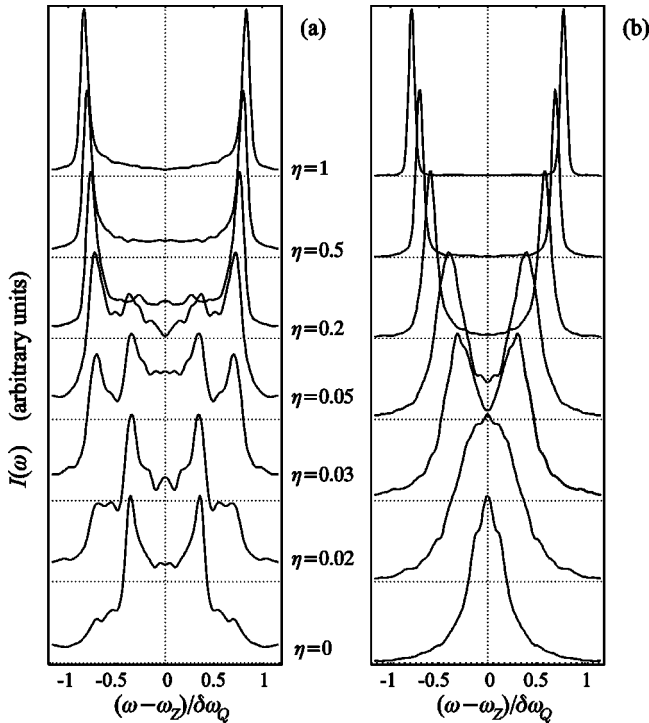
FIG. 4. ^{2}H NMR spectra of the radial droplet in the nematic phase at $T^*=0.8$ for different values of η; no-diffusion limit (a), fast diffusion limit (b). A hedgehog-to-axial structural transition occurs with increasing η. All spectra have been normalized so as to obtain same peak heights.

ness of this region is again roughly equal to the field coherence length ξ. In the intermediate regime with $0<\eta<0.2$ the spectra are composed both of the Pake type contribution originating from the surface layers and of two narrow peaks being a signature of the field-ordered core. With increasing η
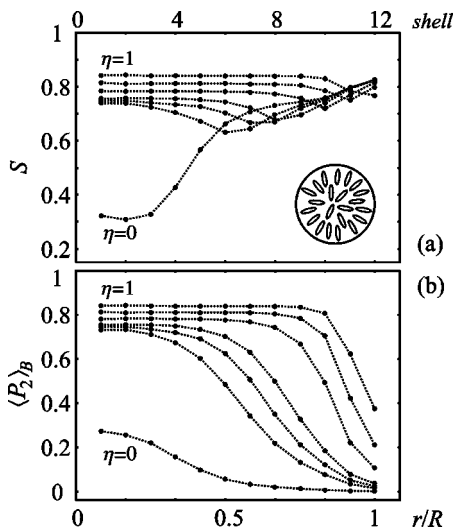

FIG. 5. Order parameters calculated for the radial droplet at $T^*=0.8$ (nematic phase): (a) standard nematic (S) and (b) external field ($\langle P_2 \rangle_B$) order parameter as a function of the distance from the droplet center. Curves are plotted for (top to bottom): $\eta=1$, $\eta=0.5$, $\eta=0.2$, $\eta=0.05$, $\eta=0.03$, $\eta=0.02$, and $\eta=0$, respectively. The defect core transforms into an aligned structure. The molecular alignment for $\eta=0$ is depicted schematically as inset.

TABLE II. Radial droplet at $T^*=0.8$: comparison of S and $\langle \omega_Q \rangle$ deduced from NMR spectra with those calculated directly from Monte Carlo data.

η	S_{peak}	S_{MC}	$(\langle \omega_Q \rangle / \delta \omega_Q)_{peak}$	$(\langle \omega_Q \rangle / \delta \omega_Q)_{MC}$
0.0	0.72 ± 0.02	0.73 ± 0.10	0	0.03
0.02	0.70 ± 0.02	0.73 ± 0.08	0	0.02
0.03	0.70 ± 0.02	0.74 ± 0.08	0.31	0.28
0.05	0.70 ± 0.01	0.74 ± 0.08	0.40	0.36
0.2	0.77 ± 0.01	0.76 ± 0.065	0.59	0.57
0.5	0.80 ± 0.01	0.79 ± 0.06	0.70	0.70
1.0	0.84 ± 0.01	0.82 ± 0.05	0.78	0.78

the latter contribution prevails, as it is clearly evident from Fig. 4(a). Again it is possible to check the agreement of values for S deduced from peak positions and from MC data (Table II).

In the fast diffusion regime the spectrum of the radial droplet for $\eta=0$ consists of a single line located at $\langle \omega_Q \rangle = 0$ since the molecular orientational distribution is spatially isotropic [2,29]. As soon as there is a preferred direction (as in the bipolar case or in a strong field), $\langle \omega_Q \rangle = 0$ no longer holds and the spectrum splits into two narrow and symmetric peaks. Figure 4(b) shows the fast diffusion spectra for radial boundary conditions. As expected, we observe a single line in the spectrum only if the external field is off or relatively weak with $\eta \lesssim 0.02$. Increasing the field strength, the spectrum gradually transforms into the two-peak pattern described above. For a comparison of peak positions and $\langle \omega_Q \rangle$ calculated from MC data see Table II; the agreement of the two estimates is fairly good.

C. Spectra above nematic-isotropic transition

In the following we will consider both types of boundary conditions at $T^*=1.2$, a higher temperature already above the nematic-isotropic transition. Molecular motion in the bulk isotropic phase is spatially isotropic (i.e., there is no long-range orientational order), hence we have $S=0$. Consequently, the quadrupolar perturbative contribution to the deuteron energy levels is averaged out and the frequency splitting $\omega_Q \propto S$ vanishes [see Eq. (2)]. In this case a single line positioned at $\omega_Q=0$ appears in the NMR spectrum.

Consider the bipolar droplet for $\eta=0$ first: the corresponding spectrum consists of a single line at zero splitting, as expected [Fig. 6(a)]. A calculation of the nematic scalar order parameter S [Fig. 7(a)] reveals some residual bipolar ordering with $S>0$ in the outer molecular layers, which is responsible for a rather large line width. Applying the external field, the two peaks characteristic for ordered nematic phases reappear. Also the nonzero values of both order parameters (S and $\langle P_2 \rangle_B$) given in Fig. 7 are restored again. All these observations show that a strong enough external field can overwhelm temperature effects and induce nematiclike molecular ordering also above the nematic-isotropic transition temperature [9,10], which has been observed also experimentally [30]. Like in the nematic phase, the quadrupolar splitting increases with increasing η. Again, peak positions and MC-data values for S match (see Table III). We can also compare the peak positions (and, simultaneously,
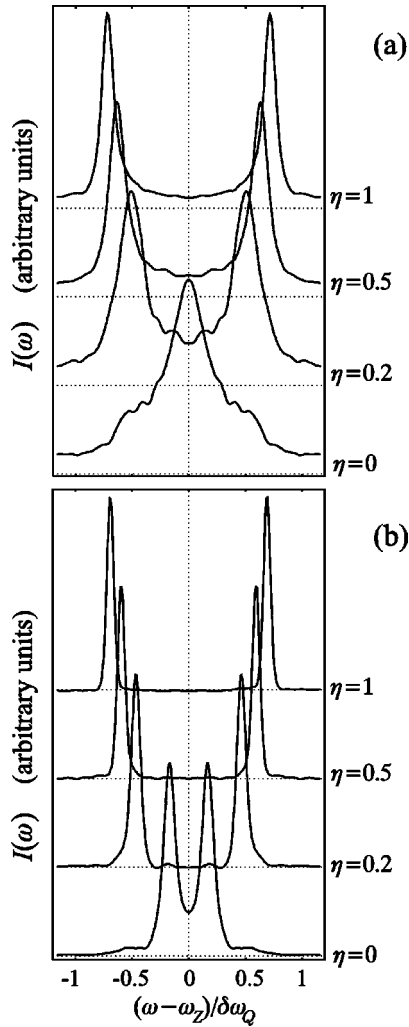
FIG. 6. Bipolar droplet; same as Fig. 2, but at $T^* = 1.2$ above the nematic-isotropic (NI) transition temperature. For strong enough fields a nonzero quadrupolar splitting is restored.
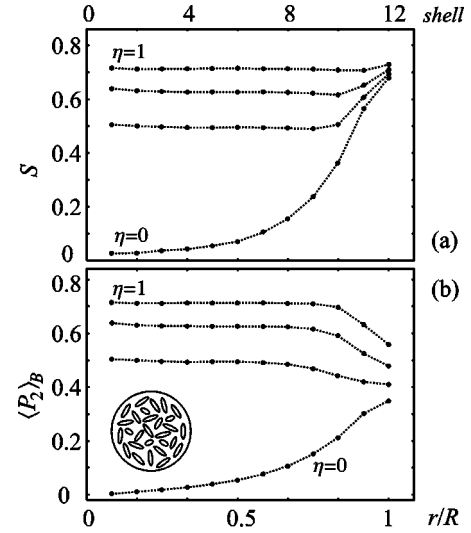

FIG. 7. Bipolar droplet; same as Fig. 3, but at $T^* = 1.2$ (above the NI transition temperature). Even for $\eta = 0$ there is some residual surface-induced nematic order in the outer layers of the droplet, while in a strong enough external field nematic order is restored throughout the droplet.

induced nematic ordering above T_{NI}. A comparison of peak position-determined S and MC-calculated S given in Table IV again shows that the agreement of the two values is fairly good. As with the bipolar droplet, one can compare these values with those obtained at $T^* = 0.8$ in the nematic phase and again find that the degree of nematic ordering is lower at a higher temperature. Finally, Fig. 8(b) shows the corresponding fast diffusion limit spectra. For $\eta = 0$ the line is single-peaked in spite of residual order with nonzero S close to the surface (see Fig. 9). Note, however, that in this layer we are dealing with radial order yielding $\langle \omega_Q \rangle = 0$ already in itself. In other cases with external field, two peaks reappear and the corresponding splitting increases with η. The agreement of $\langle \omega_Q \rangle$ evaluated from peak positions and from MC data is very good again; see Table IV.

D. Final remarks

Finally, it is necessary to stress that simulating translational diffusion, we simply assumed the diffusive process to be isotropic and spatially homogeneous. As reported in Ref. [8], taking into account the anisotropy of the diffusion tensor does not affect the calculated NMR spectra significantly. On

the estimates for S) with those obtained for the lower temperature $T^* = 0.8$. As expected, for $T^* = 1.2$ the estimated values for S are lower than those for $T^* = 0.8$ (see above). This suggests that although rather strong, the external field is still not the only important element in determining the structure inside the droplet and that disordering temperature-induced effects are still well-pronounced. In the fast diffusion limit, all spectra, including that for $\eta = 0$, consist of two peaks since $\langle \omega_Q \rangle \neq 0$ [see Fig. 6(b)]. This result is expected for $\eta \neq 0$ and also for $\eta = 0$, where the ordering effect of the external field is absent, but there is residual surface-induced ordering [for the behavior of S see Fig. 7(a)]. Checking the matching of peak positions and the MC-deduced values of $\langle \omega_Q \rangle$, the agreement is still very good (Table III).

Repeating the analysis for radial boundary conditions and $T^* = 1.2$ gives similar results: in the no-diffusion limit the single broad peak centered at $\omega_Q = 0$ for $\eta = 0$ splits into a doublet for $\eta \neq 0$ and the splitting increases with η [see Fig. 8(a)]. If the field is absent, the order parameters S and $\langle P_2 \rangle_B$ plotted in Fig. 9 show the existence of residual radial order in the surface layers of the droplet, while in the core the liquid crystal is isotropic. For nonzero η both order parameters acquire a nonzero value and hence again confirm field-

TABLE III. Bipolar droplet at $T^* = 1.2$: comparison of S and $\langle \omega_Q \rangle$ deduced from NMR spectra with those calculated directly from Monte Carlo data. S_{MC} for $\eta = 0$ is not given since in the isotropic phase the method we employed to calculate S results in an overestimate because in a disordered phase the nematic director is not well-defined [33].

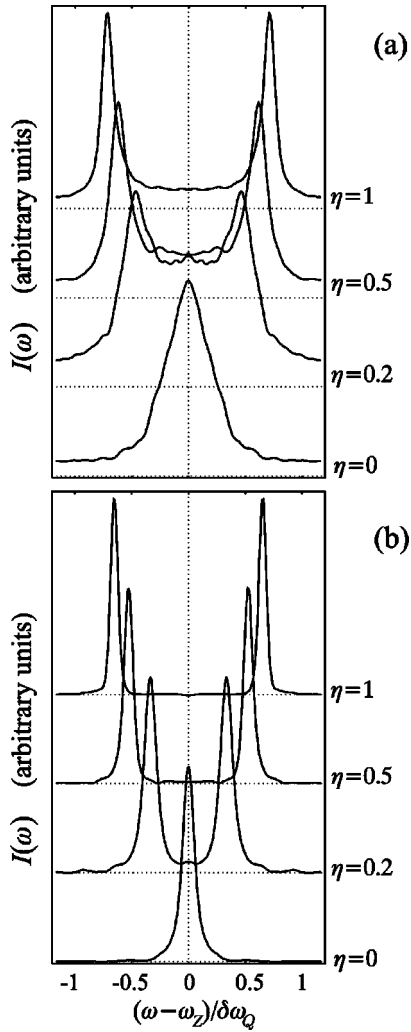| η	S_{peak}	S_{MC}	$(\langle \omega_Q \rangle / \delta \omega_Q)_{peak}$	$(\langle \omega_Q \rangle / \delta \omega_Q)_{MC}$
0.0	0		0.17	0.18
0.2	0.51 ± 0.01	0.53 ± 0.08	0.46	0.46
0.5	0.63 ± 0.01	0.63 ± 0.05	0.59	0.60
1.0	0.72 ± 0.01	0.71 ± 0.03	0.69	0.69

FIG. 8. Radial droplet; same as Fig. 4, but at $T^* = 1.2$ above the NI transition. Again, for strong enough fields a nonzero quadrupolar splitting is restored.

the other hand, once a molecule diffuses into the first surface molecular layer, it may experience a slowdown in its translational motion, as seen in several experimental studies [31,32]. This spatial inhomogeneity in the diffusive process can become important for the calculation of the spectra, especially if the molecular surface dwell time is long and if the molecular exchange between the bulk and the surface layer is accompanied by a significant change in the degree of nematic order or in molecular orientation.

Note also that our calculation of NMR spectra starting from MC simulations can easily be applied to any type of geometric confinement. Therefore it is advantageous with respect to calculations based on the elastic continuum theory where the determination of the equilibrium director field may become nontrivial if one is dealing with complicated boundary conditions.

Experimentally, ^{2}H NMR has been applied to study mostly PDLC samples with planar anchoring, resulting in bipolar droplets [2,5,13,22,23]. The spectra available from these analyses either consist of two well-distinguished peaks or are equivalent to the Pake-type powder pattern. In the former case, all bipolar droplet symmetry axes were aligned along a given direction prior to recording the NMR spectrum
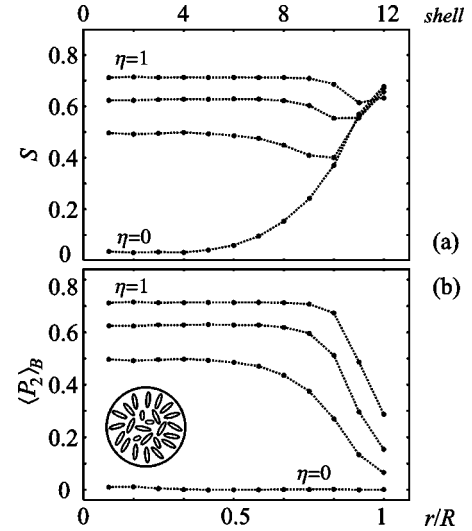

FIG. 9. Radial droplet; same as Fig. 5, but at $T^* = 1.2$ above the NI transition. Again, for $\eta = 0$ there is residual surface-induced nematic order persisting in the outer layers of the droplet, while in a strong enough external field nematic order is restored throughout the droplet.

(e.g., by a strong field during the droplet formation), which corresponds to the case analyzed here. The qualitative agreement of the calculated and experimental spectra is then good. Unfortunately, analyses performed in external fields [5,13] were devoted to molecular reorientation inside droplets, requiring a setup with the spectrometer and external field perpendicular to each other, which does not match with the setup in our analysis where both fields are parallel. On the other hand, if there is no strong field to align the bipolar symmetry axes, they are distributed over the whole solid angle and this then results in a Pake-type spectrum [5,22,23]. Although we simulated only one droplet, we can reproduce this result by assuming a distribution of spectrometer field directions, keeping the bipolar symmetry axis of the droplet fixed, and superimposing the corresponding spectra. Since the resulting overall spectrum is similar to the familiar Pake-type pattern, as obtained also for radial droplets, we do not display it here again.

For a more serious quantitative comparison of the calculated spectra with the experimental ones, usually recorded for larger droplets than those studied here, it would be necessary to simulate droplets containing a significantly larger number of spins, so as to access radii of the order of ~ 1 μm. Moreover, it turns out that the distribution in orientations of droplet symmetry axes is closely related to the shape of the droplets, which is not necessarily spherical—as

TABLE IV. Radial droplet at $T^* = 1.2$: comparison of S and $\langle \omega_Q \rangle$ deduced from NMR spectra with those calculated directly from Monte Carlo data. As in Table III, S for $\eta = 0$ is not given.

η	S_{peak}	S_{MC}	$(\langle \omega_Q \rangle / \delta \omega_Q)_{peak}$	$(\langle \omega_Q \rangle / \delta \omega_Q)_{MC}$
0.0	0		0	0.001
0.2	0.46 ± 0.01	0.48 ± 0.11	0.33	0.34
0.5	0.62 ± 0.01	0.59 ± 0.08	0.52	0.52
1.0	0.71 ± 0.01	0.68 ± 0.08	0.65	0.65

assumed so far—but rather somewhat ellipsoidal, which reflects in NMR spectra as well [13]. However, considerations of all these phenomena are already beyond the scope of this paper's goal which is merely to show how basic mechanisms driving the molecular ordering inside nematic droplets reflect in NMR spectra.

IV. CONCLUSION

In this paper, we have calculated ^{2}H NMR spectra of nematic droplets, as found in polymer-dispersed liquid crystalline (PDLC) materials. The method applied for this purpose allowed us to include dynamic phenomena such as fluctuations of molecular long axes and translational diffusion in the calculation of the spectra. The input data for the calculation were provided from Monte Carlo simulations based on the simple Lebwohl-Lasher lattice model. Simulating nematic configurations inside a PDLC droplet, special attention was paid to the effect of the external field. It both aligns nematic molecules (changes their average orientation) and increases the degree of nematic order. These conclusions, drawn from MC data by calculating appropriate order parameters, reflect also in the resulting NMR spectra. In the analysis, we considered droplets with bipolar and radial boundary conditions. The simulated spectra are different for the two cases, especially for low values of the external field, and can be used to discriminate between different molecular organizations. In the radial case the external field induces a continuous structural transition from the radial ''hedgehog'' structure to an aligned one whose NMR spectrum becomes similar to that of the bipolar droplet. Further, an external field of sufficient strength can induce nematic ordering even at temperatures above the nematic-isotropic transition.

[1] G. P. Crawford and S. Žumer, *Liquid Crystals in Complex Geometries Formed by Polymer and Porous Networks* (Taylor and Francis, London, 1996).

[2] A. Golemme, S. Žumer, J. W. Doane, and M. E. Neubert, Phys. Rev. A **37**, 559 (1988).

[3] R. Ondris-Crawford, E. P. Boyko, B. G. Wagner, J. H. Erdmann, S. Žumer, and J. W. Doane, J. Appl. Phys. **69**, 6380 (1991).

[4] P. Drzaic, Mol. Cryst. Liq. Cryst. **154**, 289 (1988).

[5] R. Aloe, G. Chidichimo, and A. Golemme, Mol. Cryst. Liq. Cryst. **203**, 1155 (1991).

[6] C. Chiccoli, P. Pasini, F. Semeria, E. Berggren, and C. Zannoni, Mol. Cryst. Liq. Cryst. **266**, 241 (1995).

[7] *Advances in the Computer Simulations of Liquid Crystals*, edited by P. Pasini and C. Zannoni (Kluwer, Dordrecht, 2000).

[8] C. Chiccoli, P. Pasini, G. Skačej, C. Zannoni, and S. Žumer, Phys. Rev. E **60**, 4219 (1999).

[9] E. Berggren, C. Zannoni, C. Chiccoli, P. Pasini, and F. Semeria, Phys. Rev. E **49**, 614 (1994).

[10] E. Berggren, C. Zannoni, C. Chiccoli, P. Pasini, and F. Semeria, Phys. Rev. E **50**, 2929 (1994).

[11] P. A. Lebwohl and G. Lasher, Phys. Rev. A **6**, 426 (1972).

[12] P. G. de Gennes and J. Prost, *The Physics of Liquid Crystals* (Clarendon Press, Oxford, 1993).

[13] M. Ambrožič, P. Formoso, A. Golemme, and S. Žumer, Phys. Rev. E **56**, 1825 (1997).

[14] C. Chiccoli, P. Pasini, F. Semeria, and C. Zannoni, Phys. Lett. A **150**, 311 (1990); C. Chiccoli, P. Pasini, F. Semeria, and C. Zannoni, Mol. Cryst. Liq. Cryst. **212**, 197 (1992).

[15] C. Chiccoli, P. Pasini, F. Semeria, and C. Zannoni, Mol. Cryst. Liq. Cryst. **221**, 19 (1992).

[16] E. Berggren, C. Zannoni, C. Chiccoli, P. Pasini, and F. Semeria, Chem. Phys. Lett. **197**, 224 (1992).

[17] N. Priezjev and R. A. Pelcovits, ar Xiv e-print cond-mat/0006240.

[18] L. M. Blinov, A. Yu. Kabayenkov, and A. A. Sonin, Liq. Cryst. **5**, 645 (1989).

[19] N. Metropolis, A. W. Rosenbluth, M. N. Rosenbluth, A. H. Teller, and E. Teller, J. Chem. Phys. **21**, 1087 (1953).

[20] U. Fabbri and C. Zannoni, Mol. Phys. **58**, 763 (1986).

[21] J. A. Barker and R. O. Watts, Chem. Phys. Lett. **3**, 144 (1969).

[22] A. Golemme, S. Žumer, D. W. Allender, and J. W. Doane, Phys. Rev. Lett. **61**, 2937 (1988).

[23] J. Dolinšek, O. Jarh, M. Vilfan, S. Žumer, R. Blinc, J. W. Doane, and G. Crawford, J. Chem. Phys. **95**, 2154 (1991).

[24] R. Y. Dong, *Nuclear Magnetic Resonance of Liquid Crystals* (Springer-Verlag, New York, 1994).

[25] A. Abragam, *The Principles of Nuclear Magnetism* (Clarendon Press, Oxford, 1961).

[26] S. Žumer, P. Ziherl, and M. Vilfan, Mol. Cryst. Liq. Cryst. **292**, 39 (1997).

[27] C. Zannoni, in *The Molecular Physics of Liquid Crystals*, edited by G. R. Luckhurst and G. W. Gray (Academic, London, 1979), Chap. 9.

[28] I. Lelidis, M. Nobili, and G. Durand, Phys. Rev. E **48**, 3818 (1993).

[29] S. Kralj, M. Vilfan, and S. Žumer, Liq. Cryst. **5**, 1489 (1989).

[30] I. Lelidis and G. Durand, Phys. Rev. E **48**, 3822 (1993).

[31] G. P. Crawford, D. K. Yang, S. Žumer, D. Finotello, and J. W. Doane, Phys. Rev. Lett. **66**, 723 (1991).

[32] M. Vilfan, G. Lahajnar, I. Zupančič, S. Žumer, R. Blinc, G. P. Crawford, and J. W. Doane, J. Chem. Phys. **103**, 8726 (1995).

[33] C. Zannoni, J. Chem. Phys. **84**, 424 (1986).